Static and Dynamic Precipitation Behavior of the Al–20wt.% Zn Alloy *

Chong-Yu Liu(刘崇宇)[1,2**], Hong-Jie Jiang(江鸿杰)[1], Chun-Xia Wang(王春霞)[1], Hai-Quan Qi(亓海全)[1], Yi-Bing Li(李义兵)[1,3], Ming-Zhen Ma(马明臻)[2], Ri-Ping Liu(刘日平)[2]

[1]*Key Laboratory of New Processing Technology for Nonferrous Metal & Materials (Ministry of Education), Guilin University of Technology, Guilin 541004*

[2]*State Key Laboratory of Metastable Materials Science and Technology, Yanshan University, Qinhuangdao 066004*

[3]*Guangxi Key Laboratory of Universities for Clean Metallurgy and Comprehensive Utilization of Nonferrous Metal Resources, Guilin 541004*

(Received 26 February 2016)

The static and dynamic precipitation behavior of solution-treated binary Al–20 wt.% Zn alloy is investigated via artificial aging, cold rolling and artificial aging combined with cold rolling. The solution-treated Al–Zn alloy exhibits high thermal stability during aging, and low densities of nano-sized Zn particles are precipitated along with Al grain boundaries after aging at 200°C for 13 h. Compared with static precipitation, dynamic precipitation occurs more easily in the Al–Zn alloy. Zn clusters are obtained after cold rolling at an equivalent plastic strain of 0.6, and the size of the Zn phase reaches hundreds of nanometers when the strain is increased to 12.1. The results show that the speed of static precipitation can be significantly enhanced after the application of 2.9 rolling strain. Grain refinement and defects induced by cold rolling are considered to promote Zn precipitation. The hardness of Al–Zn alloy is also affected by static and dynamic precipitations.

PACS: 61.46.−w, 61.46.Bc, 61.72.Cc, 66.30.Lw DOI: 10.1088/0256-307X/33/5/056101

Precipitation behavior is crucial to the improvement of properties of metals.[1,2] The static precipitation behavior of age-hardenable Al alloys has been widely investigated for nearly a century. The static precipitation is usually produced by treating solutions below liquid temperatures, quenching and then aging at elevated temperatures, which are usually in the range 100–200°C.[2]

Recently, dynamic precipitation has been detected during deformation.[3−13] Compared with static precipitation, dynamic precipitation requires less time and occurs at lower temperatures because of the faster diffusion velocity of solute atoms in the Al matrix.[3] Deformation leads to loss of the low-energy interface between precipitates and Al matrix, thus the growth orientation of precipitates triggered by dynamic precipitation is different from that caused by static precipitation.[4] Furthermore, dynamic precipitation was found in some 'non-age-hardenable' alloys such as Al–Mg systems.[5]

Dynamic precipitation always plays an important role in microstructures and properties of Al alloys. For example, the segregation of solutes at grain boundaries (GBs) during high-pressure torsion can enhance grain refinement of Al alloys.[6] Dynamic precipitation can improve the ductility of ultrafine-grained (UFG) Al alloys,[7,8] can enhance the electrical conductivity of high-strength Al alloys,[9] and can soften some Al alloys.[10,11]

A systematic comparison between static and dynamic precipitations of Al alloy is necessary to understand the effects of GBs, dislocations and vacancies on the diffusion of solute atoms in the Al matrix. In this study, a supersaturated solid solution Al–Zn alloy that decomposes easily during deformations[8,10−14] is used as the raw material to investigate the static and dynamic precipitation behavior of Al alloy. The effects of static and dynamic precipitation on the hardness of the Al–Zn are also investigated.

Al–20 wt.% Zn alloy was prepared by melting high-purity components in a vacuum. The castings were cut into 16 mm × 80 mm × 200 mm samples, solution-treated at 550°C for 3 h and quenched in water. Three routes were used for subsequent processing, that is, (i) aged at 200°C for 0.5–13 h; (ii) rolling from 16–0.5 mm, with 10 cycles of accumulative roll bonding used to obtain larger deformation degree, and the equivalent plastic strain ε reaching up to ∼12.1; and (iii) rolling from 16–1.3 mm (ε is about 2.9) and aging at 100 and 200°C for 0.5–10 h. All of the rolling process was performed at room temperature.

The phase structures of the Al–Zn samples were determined by x-ray diffraction (XRD). The microstructures were examined by using transmission electron microscopy (TEM), and TEM images were taken from rolling direction-transverse direction planes. The TEM specimens were prepared via twin-jet electrochemical polishing in a solution containing

*Supported by the National Basic Research Program of China under Grant No 2013CB733000, the Natural Science Foundation of Guangxi Province under Grant No 2015GXNSFBA139238, and the Guangxi 'Bagui' Teams for Innovation and Research.

**Corresponding author. Email: lcy261@glut.edu.cn

© 2016 Chinese Physical Society and IOP Publishing Ltd

7% perchloric acid and 93% methanol at 16 V and −10℃. Observations were performed at 200 kV in a JEM2010 microscope. Hardness measurement was conducted by using a Vickers microhardness tester (using 9.8 N load for 15 s).

Figure 1(a) shows the XRD of solution-treated (as-SS) Al–Zn alloy aged at 200℃ for different times. The Zn peak was not observed in all the samples, and the Al peaks did not shift during aging, as shown by the inset in Fig. 1(a). Figure 1(b) shows the continuously increasing intensity of Zn peaks and shift towards low-angle orientation of Al peaks, as shown by the inset in Fig. 1(b).

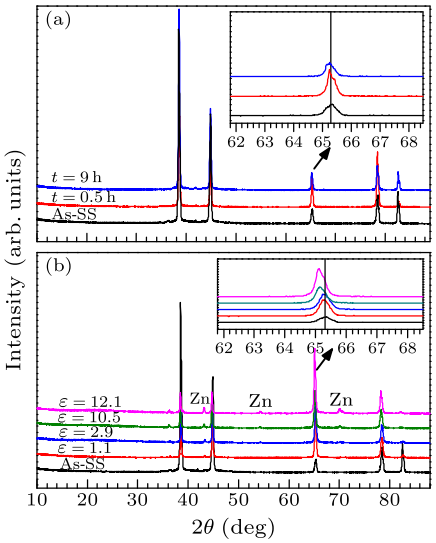

Fig. 1. XRD of As-SS Al–20% Zn alloy (a) aged at 200℃ for different times and (b) rolled after different strains.

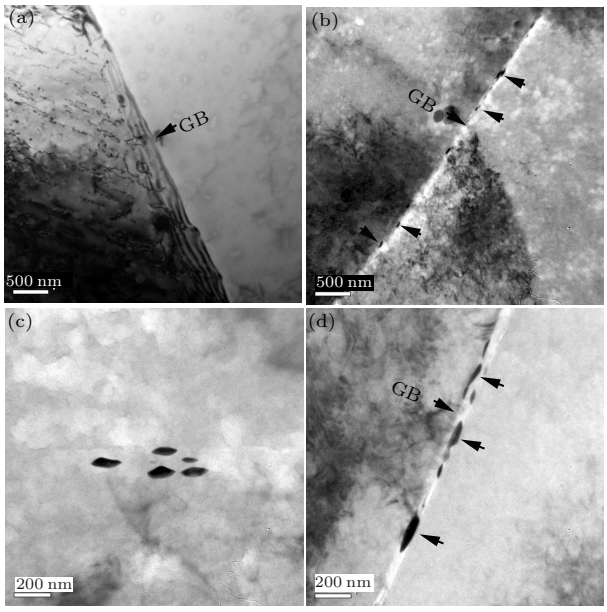

Fig. 2. (a) The TEM image of the as-SS Al–Zn alloy, and the TEM images of the as-aged Al–20% Zn alloy performed at 200℃ for (b) 0.5 h, (c) 0.5 h and (d) 13 h. Arrows denote the precipitates.

Figure 2(a) shows that the grain size of the as-SS Al–Zn alloy is significantly large so that a whole grain could not be observed in the field of vision. The as-SS sample is characterized by the absence of precipitates, low density of dislocations and well-defined GBs. Figures 2(b) and 2(c) show that precipitates with sizes below 50 nm are obtained along the GBs after aging at 200℃ for 0.5 h. By increasing the aging time to 13 h, the size of the precipitates increases to 200 nm. The precipitate phase agglomerate on the GBs is shown in Fig. 2(d).

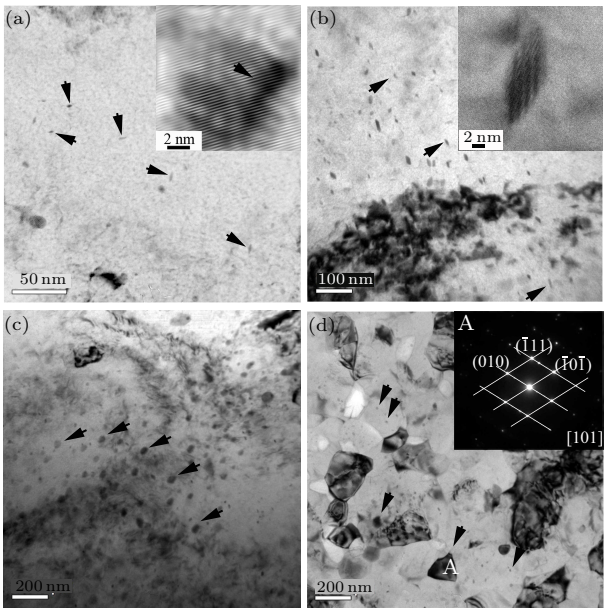

Fig. 3. TEM images of rolled Al–20% Zn alloy with strains of (a) 0.6, (b) 1.1, (c) 2.9 and (d) 12.1. A Zn particle is labeled by A and the selected area diffraction pattern does correspond to this specific particle and the hcp Zn crystallographic structure. Arrows denote the precipitates.

Figure 3 shows the microstructure of rolled Al–Zn alloy with different strains. Room-temperature rolling under a small degree of deformation (0.6) induces the formation of Zn clusters with sizes below 5 nm in the Al grain interior (Fig. 3(a)). The fast Fourier transformation of high-resolution transmission electron microscope images shows no mismatch of the lattice planes between precipitate and Al matrix, suggesting coherency between the Al matrix and precipitate. Thus the precipitates in this sample are Zn atom-rich region (clusters). The precipitates with 10–25 nm sizes are obtained when the rolling strain increases to 1.1 (Fig. 3(b)). Periodic moiré fringes appear in the precipitate, suggesting that the Zn phase precipitates from Al lattice. By increasing the strain to 2.9 as shown in Fig. 3(c), the precipitates coarsen to 30 nm, and a high density of dislocations is also observed in this sample. Figure 3(d) shows that two types of Zn particles are present in the Al–Zn alloy after rolling with a strain of 12.1. Type 1 is found

within the Al grains and measured below 15 nm in size, whereas type 2 is located at the triple junctions of the Al grains and measured 50–150 nm in size. The grain size of the Al matrix is also reduced to 150 nm with considerably low dislocation density. Recrystallization is completed, and a UFG structure is obtained in this Al–Zn alloy.

Figure 4 shows the microstructure of the 2.9-strain-rolled Al–20 wt.% Zn alloy after being subjected to different aging conditions. In addition to the precipitates with equiaxed shapes that precipitated during rolling, precipitates with several nanometers are also observed within the Al grains after aging at 100℃ for 30 min (Fig. 4(a)). When the aging time is increased to 10 h, the precipitates coarsen and equiaxed shapes are assumed (Fig. 4(b)). After aging at 200℃ for 1 h, the equiaxed precipitates 50–200 nm in size are located at the triple junctions of the Al grains (Fig. 4(c)). When the aging time is increased to 10 h at 200℃, the Zn layers with several nanometers wide are obtained between the Al grains as shown in the TEM dark-field image (Fig. 4(d)).

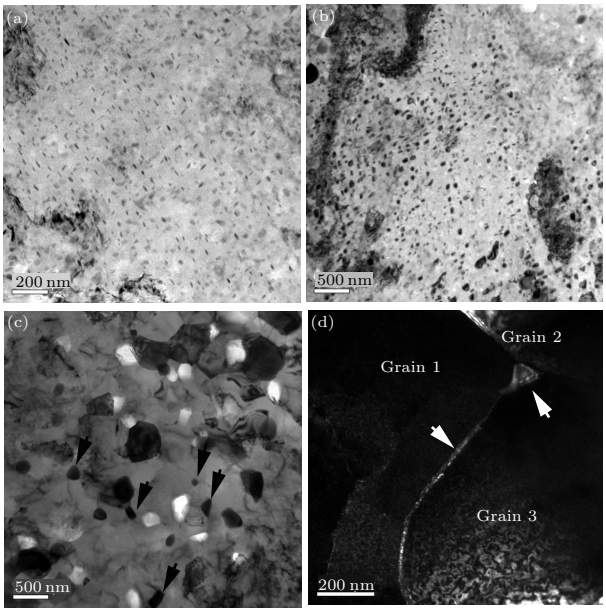

Fig. 4. TEM images of rolled Al–20 wt.% Zn alloy under different aging conditions: (a) 100℃ for 0.5 h, (b) 100℃ for 10 h, (c) 200℃ for 1 h and (d) 200℃ for 10 h. Arrows denote the precipitates.

The as-SS Al–Zn alloy shows high thermal stability during aging at 200℃ due to the coarse grain structure and minimal crystal defect. Cold rolling leads to Al grain refinement, and more vacancies and dislocations are obtained in the matrix during deformation. These crystal defects provide more nucleation sites for the Zn phase. Furthermore, the solute atoms could be dragged by deformation-induced vacancies during deformation,[5] allowing the dynamic precipitation to occur more easily in the Al–Zn alloy. Figure 4 shows that the deformation-induced crystal defects also promote the precipitation during the subsequent aging. Non-equilibrium GBs in the deformation-processed Al alloys always exhibit a crystal lattice distortion zone with several nanometers in width,[2] and high density or a fast growth of Zn particles at those GBs lead to a full coverage of GBs during aging.

Figure 5 shows the hardness of Al–20 wt.% Zn alloy during aging and rolling. The hardness of as-SS Al–Zn alloy slightly increases along with the aging time due to the precipitation strengthening (Fig. 5(a)). The rolled Al–Zn alloy shows peak hardness value (119 HV) at a strain of 2.9, as shown in Fig. 5(b). The sample is strengthened by the high density of dislocations, nano-sized Zn precipitates and solid atoms (Fig. 3(c)). It is worth mentioning that the solid solution hardening effect of Zn atom is low due to the low interaction between the Zn atom and dislocations.[15] The hardness of the 2.9-strain sample is continuously reduced with the increasing strain or the aging temperature/time, and is reduced to the value of as-SS Al–Zn alloy after aging at 200℃ for 10 h or 12.1 rolling strain.

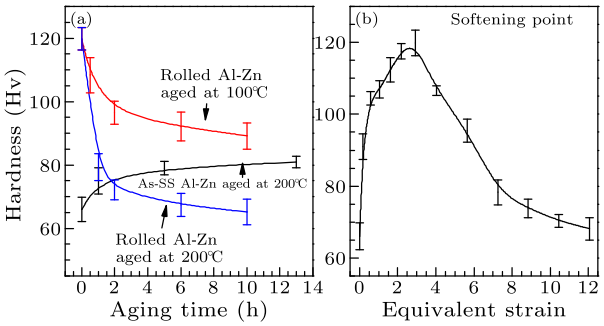

Fig. 5. Variation of Vickers hardness with (a) aging time and (b) rolling strain for the Al–20 wt.% Zn alloy.

Dynamic recrystallization or recrystallization behavior respectively caused by rolling and aging leads to grain refinement in the Al–Zn alloy. However, annihilation of dislocations, coarsening of precipitates and decomposition of solid solution also occur during rolling or subsequent aging (Figs. 3 and 4). The decrease in dislocation hardening, precipitation strengthening and solid solution strengthening is more pronounced than the increase of boundary hardening in the Al–Zn alloy. The net effect results in the softening of the 2.9-strain Al–Zn alloy during rolling or subsequent aging.

In summary, we have investigated the static and dynamic precipitation behavior of the Al–20% Zn alloy, and demonstrated that crystal defects such as GB, vacancy and dislocation can effectively promote the precipitation of the Zn phase. The precipitation also plays an important role in the hardness of the Al–20 wt.% Zn alloy.

References

[1] Zhuo L C, Liang S H, Wang F, Liu Y F and Xiong J C 2015 *Chin. Phys. Lett.* **32** 076102

[2] Sabirov I, Yu M and Valiev R Z 2013 *Mater. Sci. Eng.* A **560** 1

[3] Cai M, Field D P and Lorimer G W 2004 *Mater. Sci. Eng.* A **373** 65

[4] Sha G, Wang Y B, Liao X Z, Duan Z C, Ringer S P and Langdon T G 2009 *Acta Mater.* **57** 3123

[5] Sauvage X, Enikeev N, Valiev R, Nasedkina Y and Murashkin M 2014 *Acta Mater.* **72** 125

[6] Sha G, Tugcu K, Liao X Z, Trimby P W, Murashkin M Y, Valiev R Z and Ringer S P 2014 *Acta Mater.* **63** 169

[7] Ma Z Y, Liu F C and Mishra R S 2010 *Acta Mater.* **58** 4693

[8] Valiev R Z, Murashkin M Y, Kilmametov A, Straumal B, Chinh N Q and Langdon T G 2010 *J. Mater. Sci.* **45** 4718

[9] Sauvage X, Bobruk E V, Murashkin M Y, Nasedkina Y, Enikeev N A and Valiev R Z 2015 *Acta Mater.* **98** 355

[10] Mazilkin A A, Straumal B B, Rabkin E, Baretzky B, Enders S, Protasova S G, Kogtenkova O A and Valiev R Z 2006 *Acta Mater.* **54** 3933

[11] Mazilkin A A, Straumal B B, Borodachenkova M V, Valiev R Z, Kogtenkova O A and Baretzky B 2012 *Mater. Lett.* **84** 63

[12] Liu C Y, Yu L, Ma M Z, Liu R P and Ma Z Y 2015 *Philos. Mag. Lett.* **95** 539

[13] Sauvage X, Murashkin M Y, Straumal B B, Bobruk E V and Valiev R Z 2015 *Adv. Eng. Mater.* **17** 1821

[14] Liu C Y, Ma M Z, Liu R P, Yu L and Luo K 2015 *Sci. Chin. Phys. Mech. Astron.* **58** 104601

[15] Borodachenkova M, Barlat F, Wen W, Bastos A and Grácio J J 2015 *Int. J. Plast.* **68** 150